Optimization of LiNbO$_3$ photonic crystals: toward 3D LiNbO$_3$ micro-components

Nadège Courjal,[1,*] Jean Dahdah,[1] Gwenn Ulliac,[1] Pierre Sevillano,[1] Blandine Guichardaz,[1] and Fadi Baida[1]

[1]*Department of Optics, FEMTO-ST Institute, Route de Gray, 25030 Besançon Cedex, France*
*nadege.bodin@univ-fcomte.fr.

Abstract: We report easy-to-implement techniques to improve the reflectivity of LiNbO$_3$ photonic crystals within the photonic bandgap. Firstly, we show that widening the channel waveguides confines the optical modes in the vertical direction, which leads to the development of the first 2D-PhCs on Ti-indiffused LiNbO$_3$ waveguides. We also report the first optical characterization of PhCs implemented on ridge LiNbO$_3$ waveguides. The reflectivity is measured using a swept-source optical coherence tomography (OCT) system, together with the transmission spectrum. Finally we report 3D-PhCs LiNbO$_3$ fabricated by Focused Ion Beam milling on the side of ridge waveguides.

©2011 Optical Society of America

OCIS codes: (130.3730) Lithium niobate; (160.5298) Photonic crystals.

References and links

1. K. Yoshino, Y. Shimoda, Y. Kawagishi, K. Nakayama, and M. Ozaki, "Temperature tuning of the stop band in transmission spectra of liquid-crystal infiltrated synthetic opal as tunable photonic crystal," Appl. Phys. Lett. **75**(7), 932 (1999).
2. Y. Jiang, W. Jiang, L. Gu, X. Chen, and R. T. Chen, "80-micron interaction length silicon photonic crystal waveguide modulator," Appl. Phys. Lett. **87**(22), 221105 (2005).
3. N. G. R. Broderick, G. W. Ross, H. L. Offerhaus, D. J. Richardson, and D. C. Hanna, "Hexagonally poled lithium niobate: A two-dimensional nonlinear photonic crystal," Phys. Rev. Lett. **84**(19), 4345–4348 (2000).
4. M. Roussey, M.-P. Bernal, N. Courjal, D. Van Labeke, F. I. Baida, and R. Salut, and R. Salut, "Electro-optic effect exaltation on lithium niobate photonic crystals due to slow photons," Appl. Phys. Lett. **89**(24), 241110 (2006).
5. N. Courjal, S. Benchabane, J. Dahdah, G. Ulliac, Y. Gruson, and V. Laude, "Acousto-optically tunable lithium niobate photonic crystal," Appl. Phys. Lett. **96**(13), 131103 (2010).
6. M. P. Bernal, J. Amet, J. Safioui, F. Devaux, M. Chauvet, J. Salvi, and F. Baida, "Pyroelectric control of the superprism effect in a lithium niobate photonic crystal in slow light configuration," Appl. Phys. Lett. **98**(7), 071101 (2011).
7. G. W. Burr, S. Diziain, and M.-P. Bernal, "The impact of finite-depth cylindrical and conical holes in lithium niobate photonic crystals," Opt. Express **16**(9), 6302–6316 (2008), http://www.opticsinfobase.org/abstract.cfm?URI=oe-16-9-6302.
8. R. Geiss, S. Diziain, R. Iliew, C. Etrich, H. Hartung, N. Janunts, F. Schrempel, F. Lederer, T. Pertsch, and E.-B. Kley, "Light propagation in a free-standing lithium niobate photonic crystal waveguide," Appl. Phys. Lett. **97**(13), 131109 (2010).
9. G. Si, E. J. Teo, A. A. Bettiol, J. Teng, and A. J. Danner, "Suspended slab and photonic crystal waveguides in lithium niobate," J. Vac. Sci. Technol. B **28**(2), 316–320 (2010).
10. D. Marcuse, "Solution of the vector wave equation for general dielectric waveguides by the Galerkin method," IEEE J. Quantum Electron. **28**(2), 459–465 (1992).
11. F. Lacour, N. Courjal, M. P. Bernal, A. Sabac, C. Bainier, and M. Spajer, "Nanostructuring lithium niobate substrates by focused ion beam milling," Opt. Mater. **27**(8), 1421–1425 (2005).
12. J. D. Joannopoulos, S. G. Johnson, J. N. Winn, and R. D. Meade, "Photonic crystals: molding the flow of light," (Princeton University Press, 1995)
13. N. Courjal, B. Guichardaz, G. Ulliac, J.-Y. Rauch, B. Sadani, H.-H. Lu, and M.-P. Bernal, "High aspect ratio lithium niobate ridge waveguides fabricated by optical grade dicing," J. Phys. D Appl. Phys. **44**(30), 305101 (2011).

1. Introduction

Photonic crystal (PhC) structures have been widely investigated over the last two decades for both fundamental and application aspects. The fabrication of these PhCs on materials that are

strongly sensitive to external stimuli is a key step toward practical PhC-based optical processing devices. Several approaches have been proposed and demonstrated for the realization of such compact devices. One of them consists in infiltrating passive materials with liquid crystals [1]. An alternative method relies on the processing of active materials like semi-conductors which may be driven by modulation of the injection current [2].

Amongst the optically tunable materials, lithium niobate appears as a promising candidate, due to its high electro-optical, acousto-optical, and non-linear optical coefficients. In addition, the material has an ultra-high optical bandwidth that spans from 350nm to 5200nm. In 2000, Broderick et al. reported the first nonlinear 2D PhCs, and demonstrated efficient quasi-phase-matched 2nd harmonic generation by use of ferroelectric domain inversion [3]. More recently, electro-optic [4], acousto-optic [5] or pyroelectric 2D $LiNbO_3$ PhCs [6] have also been realized in ultracompact devices. All these tunable PhCs are integrated on annealed proton exchange (APE) waveguides. The photonic bandgaps that are experimentally observed in these PhCs exhibit rough spectral edges, whereas sharp bandgap edges would enable reduced driving power. This practical problem results from the conical shape of the holes and from the weak confinement of the optical guided mode [7].

To circumvent this issue, thin films of $LiNbO_3$ have been recently developed [8, 9]. These films allow a tight confinement of the optical mode in comparison with standard $LiNbO_3$ waveguides. They also avoid the requirement of deep holes. An improvement of the photonic bandgap edge sharpness is thus expected. But the fabrication of thin layers of $LiNbO_3$ is a difficult task that implies in particular ion implantation and mechanical thinning.

In this work we propose and demonstrate easy-to-implement alternative methods that improve the photonic bandgap of $LiNbO_3$ based PhCs. The first technique is based on the nanostructuration of widened conventional $LiNbO_3$ waveguides, while the second one relies on the development of nanostructured ridge waveguides. The reflectivity within the forbidden gap is exploited as a gauge for estimating and comparing the photonic behavior of the different nanostructured waveguides. It is measured using a swept-source OCT (optical coherence tomography) system, together with the large spectrum transmission response.

We finally show how our technological developments open the way for the development of 3D $LiNbO_3$ based PhCs.

2. PhCs integrated on standard $LiNbO_3$ waveguides

As mentioned above, traditional LiNbO3 waveguides are weakly confined, due to the small index contrast between the waveguide and the material. As a result, the core of the optical guided mode is located more than 1 μm far from the surface. On the other hand, the $LiNbO_3$ PhCs cannot be etched at depths larger than 1.5 μm. Indeed, the classical ways for etching the holes in LiNbO3 rely on Focused Ion Beam (FIB) milling or plasma etching techniques. Both techniques imply a conical shape of the holes, with typical aspect ratios (depth:width) of 3. If we want to improve the photonic bandgap behavior of the $LiNbO_3$ PhCs, it is necessary to increase the aspect ratio of the holes, or to improve the vertical confinement of the optical waveguides. The third and fourth sections of the paper will show ways toward the fabrication of holes with improved aspect ratios.

In this section, we propose to improve the vertical confinement of the standard waveguides by widening them. Widening the waveguide expands the optical mode in the horizontal direction. Consequently, as the total energy must be conserved, this widening leads to a confinement of the mode in the vertical direction. The FWHM (Full Width at Half Maximum) of the optical modes has been calculated using the Galerkin method [10], and the results are reported in Table 1. It is confirmed from these results that 12 μm width waveguides exhibit a slight reduction (~10%) of the vertical FWHM in comparison with 7 µm width waveguides. It is also shown in Table 1 that expanding the waveguides helps increasing their effective index. This technique has been tested successively on standard APE waveguides and on Ti-indiffused waveguides to improve the photonic bandgap performances of $LiNbO_3$ PhCs.

The same triangular lattice PhC of 15x22 holes has been written on both kinds of waveguides (see Fig. 1(a) and Fig. 2(a)). The PhC is designed to have a spectral gap between 1350 nm and 2000 nm for TE-polarized waves. The diameter of the holes is $D = 552$ nm, and the periodicity of the lattice is $a = 690$ nm. A single hole defect is introduced in the middle of the PhC pattern in order to test the possibility of achieving cavity effects at 1550 nm. The holes are patterned by focused ion beam (FIB) milling, with Ga^+ liquid metal ion source (LMIS) and 30 keV ion acceleration energy. The ions are focused with electrostatic lenses on the sample with a probe current of 50-60 pA. In these conditions, the depth of the holes is measured to be 1.5µm [11].

Table 1. Comparison of the optical modes of LiNbO₃ waveguides at 1.5 µm wavelength (X-cut Y propagating waveguides, TE polarization). The effective index, lateral FWHM, vertical FWHM and distance between core and surface are the results of numerical calculations that were performed using the Galerkin method [10]. The reflectivity is measured from the experimental transmission response.

Waveguide type	Width	Effective index	Lateral FWHM	Vertical FWHM	Distance between core and surface	Reflectivity @ 1500nm
APE	7 µm	2.141	3.4 µm	2.2 µm	1.50 µm	30%
APE	12 µm	2.143	6.0 µm	2.0 µm	1.47 µm	83%
Ti-indiffused	7 µm	2.139	5.6 µm	3.56 µm	2.68 µm	0%
Ti-indiffused	12 µm	2.142	5.6 µm	2.99 µm	2.22 µm	28%
Ridge, Ti-indiffused	6 µm	2.136	2.75 µm	2.87 µm	2.15 µm	40%

(a)   (b)
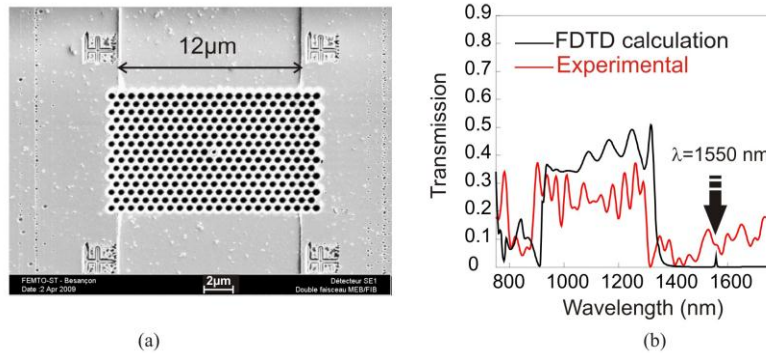
Fig. 1. LiNbO₃ PhC written on a 12 µm width APE waveguide. (a) SEM view of the PhC structure. (b) Transmission spectrum through the PhC. Black line: 2D-FDTD numerical calculation. Red line: experimental measurement (TE wave). Results obtained by normalizing the optical intensity transmitted through the nanostructured waveguide with the intensity through a single waveguide made in the same technological conditions without any PhC.

12µm

1µm

FEMTO-ST - Besançon
Date :16 Nov 2009

Détecteur SE1
Double faisceau MEB/FIB

(a)

(b)
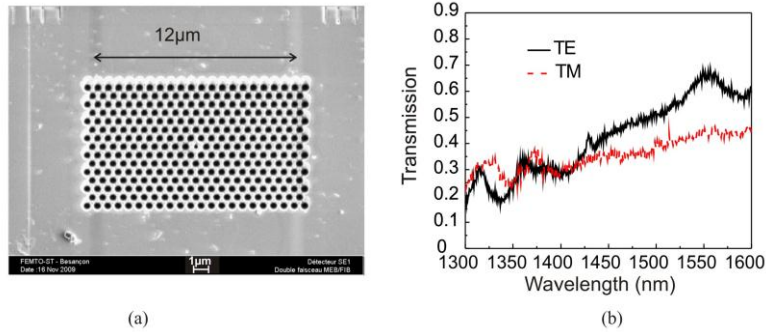
Fig. 2. LiNbO$_3$ PhC written on a 12 µm width Ti-indiffused waveguide. (a) SEM view. (b) Measured optical transmission through the PhC. Dashed red line: spectral transmission of the TM wave, solid black line: spectral transmission of the TE wave. Results obtained by normalizing the optical intensity light transmitted through the nanostructured waveguide with the intensity through a single waveguide made in the same conditions without any PhC. The linear polarization of the incident light is achieved using a fibered optical polarizer that works over the [1300-1600 nm] wavelength range.

The light is injected through a straight 7 µm width waveguide. A 1 mm long taper ensures the adiabatic transition of the fundamental guided mode between the 7 µm and the 12 µm width sections of the waveguide (see the inset of Fig. 3). The PhC is placed just at the end of the taper. The transmission response through the PhC is calculated by using 2D-FDTD homemade codes: it is represented with a black line in Fig. 1(b)).

Let us first consider the case of APE waveguides. Their fabrication is optimized in term of propagation losses and electro-optic coefficients. More precisely, the proton exchange (PE) step is achieved through a silica mask, in pure melted benzoic acid at 180°C for 1.5 hours. This step is followed by annealing at 333°C for 10 hours. The normalized transmission response through the PhC is measured by means of a LEUKOS® supercontinuum source and a Q8381 Advantest® Optical Spectrum Analyzer (OSA) as described in ref [4]. The resulting normalized transmission response is displayed in Fig. 1(b) (red line): it shows two photonic gaps with sharp band edges over the wavelength ranges of [750 nm-850 nm] and [1300 nm-1700 nm[respectively. In comparison with the 2D-FDTD calculations, the experimental gap undergoes a blue shift of 50 nm: this is due to the fabrication process, which tends to enlarge the holes at the surface of the wafer. The presented experimental result can be advantageously compared to the experimental gaps reported in references [2–4]: it confirms that enlarging the waveguides is a simple way to achieve photonic gaps with sharp walls.

In a second step we have developed an experimental setup to check the reflectivity of the PhC within the forbidden gap, at 1500nm. The PhC should behave as a perfect reflector within the bandgap [12]. Thus, the reflectivity can be used as a gauge for estimating the photonic bandgap performance of the PhC. The measurement is performed by using a tunable laser source (Photonetics® Tunics BT): the laser light is injected into the waveguide via a fibered optical circulator. The output is collected with a SMF28 fiber connected to an optical Power Meter. The reflected light is measured with the third port of the optical circulator, which is connected to the second channel of the optical Power Meter. By calculating the Fourier transform of the reflected signal, we obtain the impulse response autocorrelation reflected by the device: the result is represented in Fig. 3. In other words, this experiment is equivalent to a swept-source Optical Coherence Tomography: the peaks that can be isolated with this method reveal the presence of three different optical cavities inside the device.
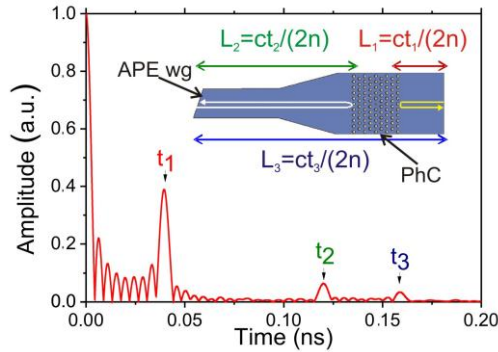
Fig. 3. Fourier transform of the reflected spectral density: impulse response correlation of the reflected light on the PhC written on an APE waveguide. Inset: schematic view of the device, and overview of the FP effects within the waveguide.

The first peak is measured at a time $t_1 = 39.2$ ps. It corresponds to the distance $L_1 = c \cdot t_1/2n_{eff}$, where $n_{eff} = 2.143$ is the guided mode effective index. The obtained numerical value $L_1 = 2.7$ mm is exactly the true distance between the PhC and the output of the waveguide (see inset of Fig. 3): it confirms that the PhC behaves as a reflector. Similar calculations show that the second (t_2) and the third (t_3) peaks of Fig. 3 correspond to Fabry-Perot (FP) effects between the entrance and the PhC ($L_2 = 8.4$mm) and between the entrance and the output of the waveguide ($L_3 = 11.1$mm $= L_1 + L_2$) respectively. The setup is not currently calibrated for measuring directly the reflectivity of the PhC. However, we can make a first estimation by exploiting the normalized transmission response: if we assume that the losses through the PhC are frequency independent, we can deduce from Fig. 1(b) that 70% of the incident light is lost through the PhC. The extinction ratio at 1500 nm is measured to be 16.7%. This means that the PhC has a reflection coefficient of almost 83% at 1500nm.

The same photonic crystal cavity has also been implemented on a standard Ti-indiffused waveguide which was fabricated with an 85 nm-thick rib of titanium diffused at 1020°C for 10 hours. A standard Ti-indiffused waveguide with a width of 7 µm is not adequate for obtaining a photonic gap: the optical mode is too buried so the coupling with the PhC mode is very weak. This feature has been experimentally verified and is summarized in Table 1 where the reflectivity for this kind of waveguide falls to 0% at 1500 nm. Nevertheless, for a wider waveguide (12 µm), a small reflection occurs as it is illustrated in Fig. 4. Indeed, the first peak of the pink curve (TE polarization) leads to a cavity length of $L_1 = ct_1/(2n_e) = 2.1$ mm corresponding to the distance between the PhC and the output of the waveguide. The other peaks can be attributed to different cavity lengths as interpreted previously for Fig. 3.
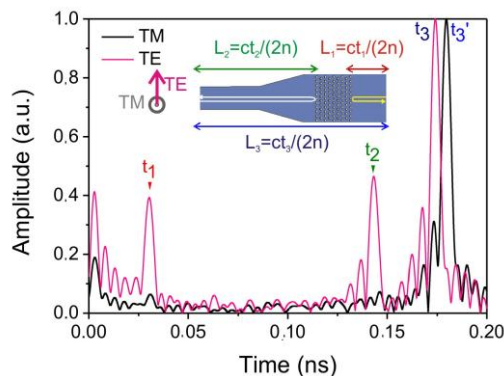
Fig. 4. PhC written on the Ti-indiffused waveguide: impulse response correlation of the reflected TE (pink line) and TM (black line) optical waves. Inset: schematic view of the device, and overview of the FP effects within the waveguide.

From the large spectrum transmission response (Fig. 2 (b), black line), we have deduced that 30% of the light is lost through the PhC, and that only 28% of the light is reflected back by the PhC at 1500 nm. Because the photonic crystals are tapered and have no vertical index confinement other than the diffused waveguide, there is a significant mismatch between the large transmission response (black line of Fig. 2(b)) and the 2D-FDTD calculations (black line of Fig. 1(b)): 3D FDTD calculations are currently being developed to verify this point.

In Ti-indiffused waveguides, both TE and TM polarizations are guided. We can observe in Fig. 4 that the TM polarization undergoes only one FP effect (black line), with a cavity length of $L_3 = ct_3'/(2n_o) = ct_3/(2n_e)$, where $n_o = 2.22$ is the effective ordinary index of the TM optical guided mode. So the TM wave is not reflected by the PhC, which is in good agreement with the PWE (Plane Wave Expansion) calculations. Indeed, the band diagram calculated for the TM wave does not show any bandgap within the wavelength range [1000nm-1700nm]. Consequently, the effect of reflection only observed with the TE polarized light confirms the presence, in this case, of a photonic bandgap effect.

This study shows that enlarging the waveguide may appear as a simple way to improve the reflectivity of the PhC. However, this trick is not convenient for the development of PhC cavities or PhC waveguides. It is indeed clear from Fig. 1(b) that there is no hope of obtaining a transmission peak through a photonic cavity if it is implemented on a large waveguide. In a second step, we have hence developed ridge waveguides for confining the optical mode in the horizontal direction. According to the 2D-FDTD calculations reported in Fig. 5, we can expect enhanced transmission of the photonic cavity peak at 1550nm.
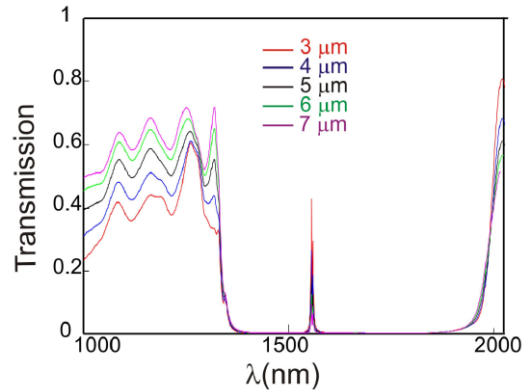
Fig. 5. Influence of the waveguide width on the transmitted spectrum. Numerical simulations (2D-FDTD) are performed for a 9x10 triangular lattice PhC of holes with a period of 690 nm and with holes' diameter of $D = 552$ nm. The cavity is made up with a single hole defect cavity at the center of the PhC.

3. PhCs integrated on ridge waveguides

The ridge waveguide is implemented on an X-cut LiNbO$_3$ wafer and is parallel to the Y direction of propagation. We first produce a Ti-indiffused planar waveguide through diffusion of an 85-mm thick layer of titanium at 1020°C for 10 hours. The ridge is then diced with a circular precision saw (DISCO DAD 321) as described in ref [13]. Finally a 9x10 lattice of holes with a period of 690 nm and with holes' diameter of $D = 552$ nm is FIB milled into the ridge (see Fig. 6(a)).
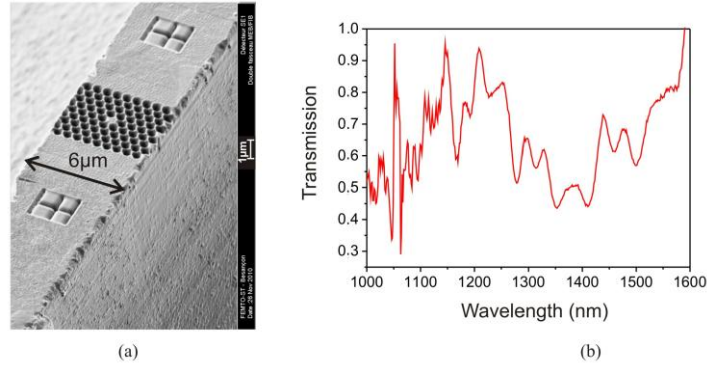
Fig. 6. PhC written on a ridge waveguide (a) SEM view. (b) Normalized spectral transmission response through the PhC.

The normalized transmission response through the PhC is reported in Fig. 6(b) for the TE polarization. From this figure we can conclude that the losses induced by the PhC have been significantly reduced by a factor of 6 in comparison with the configuration implemented on a standard waveguide: they are now estimated to be of 5%. In Fig. 6(b), an almost photonic bandgap appears between 1250 nm and 1600 nm. The extinction ratio is measured to be 60% at 1500nm, which corresponds to a reflection coefficient of 40%. This is 133% better than what was measured on a standard Ti-indiffused waveguide with a width of 12 μm. This effect is confirmed in Fig. 7 where the two first peaks of the impulse response correlation confirm the FP effect between the waveguide entrance and the PhC and between the PhC and the waveguide output respectively. Here, we have to point out a significant mismatch between the 2D-FDTD results (green line of Fig. 5) and the experimental ones. Notably, we should have expected a transmission peak due to the presence of the cavity, but the experimental response does not show any peak at 1550 nm. This disagreement is not so surprising if we consider the small index contrast provided by the Ti-indiffused planar waveguides, which does not help confining the light in the vertical direction. Thus, the ridge configuration enables an improvement of the reflection effect for Ti-indiffused waveguides, but a stronger vertical confinement is mandatory if photonic cavities or waveguides are targeted. We are currently working on ensuring this vertical confinement with an additional step of proton exchange as already mentioned in ref [13], but at the moment the strong confinement of light is achieved at the expense of the propagation losses. An alternative relies on an optimization of the aspect ratios of the photonic structures. We are currently working in that way by FIB milling the ridges structures on their edges.
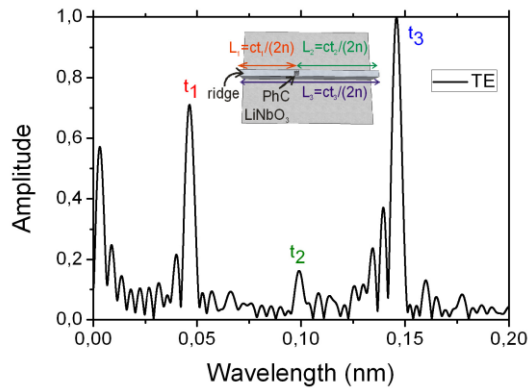
Fig. 7. PhC written on the ridge waveguide. Impulse response correlation of the reflected light. Inset: schematic view of the device, and overview of the FP effects within the waveguide.

4. PhCs on edges of ridges: toward 3D LiNbO$_3$ PhCs

The fabrication process is the same as the one mentioned above, but the ridge is tilted with an angle of 90° during the FIB milling step, so that the PhC is now engraved on the edge of the ridge. If the width of the ridge is smaller than 5 µm it is possible to etch the hole through the entire width of the ridge. Preliminary tests dedicated to the fabrication of Bragg gratings show that there is a large improvement of the aspect ratio that can be reached in comparison with those achieved by FIB milling on the surface of the waveguides. Indeed, the conical shape of the holes results from the redeposition of LiNbO$_3$ on sidewalls during the FIB milling process [11]. This redeposition is partially avoided when the beam goes through the entire width of the ridge, because a part of the milled material is evacuated at the opposite side of the ridge. This is illustrated in Fig. 8(a) and (b): the Brag gratings seen in Fig. 8 (a) result from FIB milling on top of the waveguide, whereas the Bragg gratings seen in Fig. 8 (b) have been written on the edge of the ridge. The aspect ratio (depth:width) of the grooves is improved by at least a factor 1.4 in the latter case.

(a) (b)
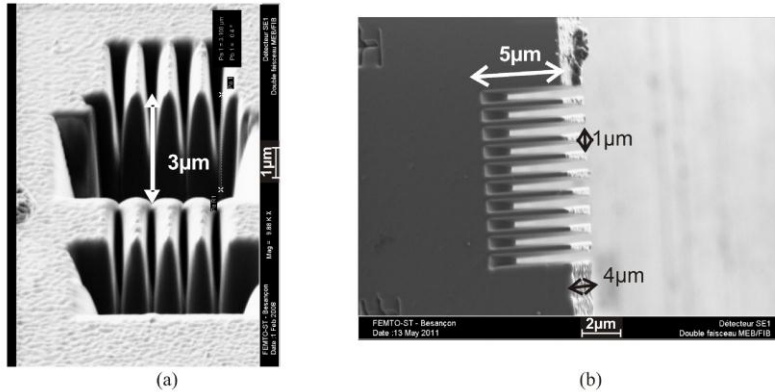
Fig. 8. SEM views of Bragg gratings patterned by FIB milling on LiNbO$_3$ optical waveguides. (a) The FIB milling is made on the top of the waveguide. (b) The FIB milling is applied on the edge of a 4 µm-width ridge.

Moreover, this approach gives promising perspectives toward the fabrication of LiNbO$_3$ 3D-PhCs, as illustrated in Fig. 9. This novel pattern has been achieved by firstly etching six grooves parallel to the top of the ridges. Then, FIB milling performed on the top of the ridge has enabled the patterning of 2D PhC on each membrane between two consecutive grooves: the FIB spot etches simultaneously all the six membranes.
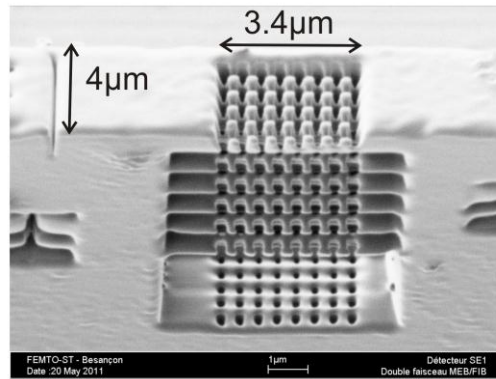
Fig. 9. SEM view of a 3D LiNbO$_3$ PhC performed on a 4µm width ridge.

5. Conclusion

PhCs made on $LiNbO_3$ waveguides have performances that strongly depend on the vertical confinement of the propagating guided mode. The reflection behavior of the PhCs in the forbidden gap has been demonstrated by means of an experimental setup that gives the spectral density of the reflected light thanks to an optical fibered circulator. The Fourier transform of this signal allows a direct observation of reflection peaks in the impulse response correlation. To our knowledge, it is the first time that swept-source OCT technique is used to characterize PhC devices. Reflection coefficient of almost 83% is reported for an APE waveguide. Moreover, we report the first demonstration of a photonic bandgap in Ti-indiffused waveguides. Enlarging a Ti-indiffused waveguide to a width of 12µm has indeed enabled to show a small photonic bandgap effect while this effect is not observed for a 7 µm width Ti-indiffused waveguide. Another approach has been tested that relies on the exploitation of ridge waveguides to improve the properties of PhCs made on $LiNbO_3$ waveguides. Finally, we have opened the way for the fabrication of a $LiNbO_3$ 3D-PhC through an original and easy-to-implement technology.